

# On electric and magnetic galvanic distortion tensor decompositions

Alan D. Chave

Woods Hole Oceanographic Institution, Woods Hole, Massachusetts

J. Torquil Smith

Institute of Theoretical Geophysics, Department of Earth Sciences, University of Cambridge, England

**Abstract.** The physics governing galvanic distortion of natural source electromagnetic induction measurements is reexamined beginning from first principles. The conditions under which a decomposition of measured magnetotelluric response tensors and magnetic transfer functions is applicable are described, and the form of the decomposition describing distortion of the electric and magnetic fields is derived directly from the integral equation defining the scattering of electric and magnetic fields by surface heterogeneities. The inclusion of magnetic field galvanic distortion leads to indeterminacy of the regional magnetotelluric response in the form of scaling by frequency-dependent, complex factors controlled by two unknown real constants. This is a generalization of the well-known static shift effect from electric field galvanic distortion and can in principle be removed if the magnitude and phase of the regional response are known at some frequency. Distortion of the magnetic transfer function is shown to be even more indeterminate, containing a term proportional to one of the regional magnetotelluric responses which is inseparably additive to the regional magnetic transfer function, as well as the complex scaling seen for magnetotellurics. A set of simultaneous nonlinear equations describing the full electric and magnetic field galvanic distortion decomposition of the magnetotelluric response tensor and magnetic transfer function is derived, and methods for their solution are described, including implementation of jackknife error estimates. The full magnetotelluric decomposition is applied to severely distorted data from the Canadian shield and seafloor data from the EMSLAB experiment. In both cases, magnetic field galvanic distortion is important at periods under a few thousand seconds. This suggests that greater attention to galvanic distortion of the magnetic field is needed during magnetotelluric surveys.

## Introduction

In recent years, the quality of magnetotelluric (MT) response function estimates has improved dramatically, both because of better instrumentation and due to the advent of robust processing methods. In many if not most instances, it has become obvious that a common electromagnetic induction scenario consists of a background one- or two-dimensional (1-D or 2-D) structure coupled with local three-dimensional (3-D) noninductive (usually called galvanic) distortion of the electric and magnetic fields. Physically, 3-D galvanic distortion is caused by the presence of electric charges at discontinuities or gradients in electrical conductivity associated with small-scale (relative to the background induction scale) surface structures. These charges will influence the observed electric field quasi-statically at all periods and

may also alter the observed magnetic field when the charges deflect regional electric currents. The 3-D surface structure causes the observed MT response function estimates to be location-dependent mixtures of the regional responses; this can include distortion of both their magnitudes and phases.

Practical analysis of MT data requires correction of observed MT responses for galvanic distortion, and considerable effort has been expended on this problem. For a recent review of the field, see *Jiracek* [1990]. In an ideal world where large electromagnetic arrays can be routinely deployed, sufficient data coverage might exist so that the surface structure can be determined along with the larger scale, regional one. This is not feasible in practice because of logistical and economic constraints. Alternately, a priori knowledge of the surface structure causing distortion would allow correction for its influence on electromagnetic data, but the necessary fine-scale information is rarely available; an exception is the seafloor study of *Tarits et al.* [1992], in which the full, complex electric and magnetic distortion tensors were computed from bathymetric data and a surface conductivity model and applied to observed MT responses.

However, MT data are more commonly collected on a coarse grid, and a more practical approach to galvanic distortion removal is based on decomposition of the observed MT response tensor into some combination of a set of distortion parameters and a 1-D or 2-D regional response tensor based on a physical distortion model. Early results include those of *Larsen* [1975, 1977] for weak distortion and *Wannamaker et al.* [1984] for more general distortion of a 1-D regional response. *Zhang et al.* [1987] extended the model of Wannamaker et al. to include regional 2-D or 3-D structures, although their detailed treatment is limited to galvanic distortion of a regional 2-D electric field by a local 2-D structure. *Bahr* [1988] considered local 3-D distortion of a 2-D structure and presented a parameterization for the tensor describing electric field distortion along with computational methods to apply it to observed MT responses.

Perhaps the most widely applied tensor decomposition is due to *Groom and Bailey* [1989]. They present a physical parameterization of the electric field distortion tensor which leads to a set of simultaneous nonlinear equations for the telluric distortion parameters and regional 2-D response functions. They further show that this approach, hereafter referred to as the Groom-Bailey (GB) decomposition, correctly recovers the regional strike and the two principal regional response functions, except for a static shift on each (i.e., multiplication by a frequency-independent real scale factor). Further comparisons of the GB decomposition with other parameterizations of the MT response tensor are given by *Groom and Bailey* [1991], while *Groom and Bahr* [1992] present a tutorial approach to recovering regional conductivity information from distorted MT responses. *Jones and Groom* [1993] showed that estimation of the regional strike in the presence of local distortion is inherently unstable and encouraged the simultaneous removal of distortion with determination of the strike direction. Finally, *Zhang et al.* [1993] considered magnetic galvanic distortion of the magnetic transfer functions and used its behavior to attempt to discriminate current channeling from induction effects.

With the exception of *Zhang et al.*, all of this work is limited in application to galvanic distortion of the electric field, although magnetic distortion effects are sometimes described briefly in principle if not in practice. Furthermore, the physical conditions under which galvanic distortion models may be applicable are often vague, reflecting the complexity of deriving a tensor decomposition from the general integral equation describing scattering of the electric and magnetic field by conductive inhomogeneities. These points, taken together with the frequent observation that galvanic distortion of the electric field alone does not adequately describe observed MT responses, especially at short periods, suggest that further examination of the problem is warranted.

In this paper, the galvanic distortion problem is reexamined beginning from first principles and the integral equations describing scattering of the electric and magnetic fields from a conductive inhomogeneity. Using an extended version of the Born approximation due to *Habashy et al.* [1993], the relevant conditions which reduce the integral equation to a tensor form like the GB decomposition are discussed and the tensor decomposi-

tion describing electric and magnetic galvanic distortion is derived. This result is applicable both to the MT response tensor and to the vertical-to-horizontal magnetic field transfer function. Magnetic field galvanic distortion decomposition leads to indeterminacy in the form of scaling of the two principal MT responses by frequency-dependent, complex factors controlled by two unknown real constants. This is analogous to static shift for electric field distortion, and methods to resolve the ambiguity are examined. The vertical-to-horizontal magnetic field transfer function decomposition is shown to be even more indeterminate in the presence of galvanic distortion, containing a term proportional to one of the regional MT responses which is inseparably additive to the regional transfer function, as well as the complex scaling of the MT case. A set of simultaneous nonlinear equations describing the full electric and magnetic field galvanic distortion decomposition is derived, and their numerical solution is described. Because of the nonlinearity of the decomposition, parametric statistical approaches toward estimating uncertainties in the decomposed MT tensor are both inherently imprecise and difficult to implement unless unreasonable approximations are used. An alternate, nonparametric jackknife procedure is advocated instead, and its practical implementation is discussed. The full MT decomposition is applied to a set of severely distorted long period MT responses from Cart Lake, Ontario, Canada. While an electric field galvanic model explains the distortion at periods longer than  $\approx 3000$  s, galvanic distortion of the magnetic field must be invoked at shorter periods. Finally, the complete MT decomposition is also applied to a single seafloor site from the EMSLAB project, and magnetic galvanic distortion is shown to be significant at periods under about two hours.

### Galvanic Distortion From First Principles

In the sequel, vectors are shown in boldface or with an overstriking arrow, while tensors are denoted by a dyad sign. The transpose of a vector or a tensor is assumed to be Hermitian (complex conjugate transpose) when the variables are complex. Vectors are assumed to be columnar, so that their transposes become row vectors.

The differential equation for the electric field under the quasistatic (pre-Maxwell) approximation in nonmagnetic media, in the absence of explicit sources, and with  $e^{-i\omega t}$  time dependence suppressed is

$$\nabla \times \nabla \times \mathbf{E}(\mathbf{r}) - i\omega\mu_0\sigma_0\mathbf{E}(\mathbf{r}) = i\omega\mu_0\delta\sigma(\mathbf{r})\mathbf{E}(\mathbf{r}) \quad (1)$$

where the symbols have their usual meaning,  $\delta\sigma(\mathbf{r})=\sigma(\mathbf{r})-\sigma_0$ , and  $\sigma_0$  refers to the background or regional conductivity structure. The solution procedure can in principle be generalized to include 1-D or 2-D background structures  $\sigma_0$ , but this requires gruesome analytical or numerical efforts, obscuring the surface distortion phenomenon which is of interest, and will not be further pursued. Because the electric field at an observation point  $\mathbf{r}$  may be in a different direction to that at a source point  $\mathbf{r}'$ , the solution of (1) must be obtained using a tensor or dyadic Green function, as described by *Yaghjian* [1980] or *Habashy et al.* [1993]. For points both internal and external to the scattering body, the electric field is described by the integral equation

$$\begin{aligned} \mathbf{E}(\mathbf{r}) = & \mathbf{E}^o(\mathbf{r}) + i\omega\mu_o \int_{V_s} d\mathbf{r}' g(\mathbf{r}, \mathbf{r}') \delta\sigma(\mathbf{r}') \mathbf{E}(\mathbf{r}') \\ & + \frac{1}{\sigma_o} \nabla \nabla \cdot \int_{V_s} d\mathbf{r}' g(\mathbf{r}, \mathbf{r}') \delta\sigma(\mathbf{r}') \mathbf{E}(\mathbf{r}') \end{aligned} \quad (2)$$

where  $V_s$  refers to the volume of the distorting body. The scalar wholospace Green function  $g(\mathbf{r}, \mathbf{r}')$  is given by

$$g(\mathbf{r}, \mathbf{r}') = \frac{e^{i\gamma_o |\mathbf{r}-\mathbf{r}'|}}{4\pi |\mathbf{r}-\mathbf{r}'|} \quad (3)$$

where  $\gamma_o = \sqrt{i\omega\mu_o\sigma_o}$ . The first term in (2) is the electric field due to the regional structure, while the second and third terms are the inductive and galvanic scattered components due to an inhomogeneity. Applying Ampere's Law to (2) gives an analogous integral equation for the magnetic induction

$$\mathbf{B}(\mathbf{r}) = \mathbf{B}^o(\mathbf{r}) + \mu_o \nabla \times \int_{V_s} d\mathbf{r}' g(\mathbf{r}, \mathbf{r}') \delta\sigma(\mathbf{r}') \mathbf{E}(\mathbf{r}') \quad (4)$$

Note that  $\mathbf{E}$  and  $\mathbf{B}$  in (2) and (4) may each contain three vector components.

The method of solution for (2) and (4) is an extension of that given by *Groom and Bahr* [1992]. A common procedure for solving (2) is based on the Born approximation in which the internal electric field in the integral terms is replaced with its background value or would at least require that the internal electric field be constant across the distorting body. These approaches involve implicit geometric conditions on the distorting body, and the Born approximation is accurate only when the difference between the internal and background electric fields is small. This led *Habashy et al.* [1993] to suggest an extension of the Born method, called the localized nonlinear (LN) approximation, in which the internal electric field behind the integral signs in (2) and (4) is replaced with

$$\mathbf{E}(\mathbf{r}') = \tilde{\mathbf{F}}(\mathbf{r}') \cdot \mathbf{E}^o(\mathbf{r}') \quad (5)$$

where the depolarization tensor is given by

$$\tilde{\mathbf{F}}(\mathbf{r}) = \left[ \tilde{\mathbf{I}} - (i\omega\mu_o \tilde{\mathbf{I}} + \frac{1}{\sigma_o} \nabla \nabla) \int_{V_s} d\mathbf{r}' g(\mathbf{r}, \mathbf{r}') \delta\sigma(\mathbf{r}') \right]^{-1} \quad (6)$$

where  $\tilde{\mathbf{I}}$  is the identity tensor. Expanding (6) in a Taylor series shows that the LN approximation accounts for multiple internal scattering in the distorting body, leading to an internal electric field which varies spatially. In the low-frequency limit, the LN approximation includes a correction for boundary charge-induced variations in the internal electric field which are not allowed under the Born approximation. *Habashy et al.* [1993] show that this leads to substantially more accurate solutions under the conditions which prevail in MT problems and will yield good results unless the conductivity contrast between the surface inhomogeneity and the regional structure is many orders of magnitude. Note that in the DC limit, (6) is real and hence the internal and background electric fields are in phase, while this condition fails when the inductive term is significant.

To solve (2) using (5), it is also expedient to assume that the background electric field is uniform across the distorting inhomogeneity and can be approximated at the

inhomogeneity by its value at the observation point  $\mathbf{r}$ . The first condition is equivalent to requiring that the inductive scale in the background medium and the source field scale be substantially greater than the largest dimension of the distorting body. The second condition is not a problem for a 1-D background model presuming source field homogeneity but might pose difficulties for more complex regional structures. Under these assumptions, (5) is replaced by

$$\mathbf{E}(\mathbf{r}') \approx \tilde{\mathbf{F}}(\mathbf{r}') \cdot \mathbf{E}^o(\mathbf{r}) \quad (7)$$

and the background field may be removed from the integral in (2) to give

$$\mathbf{E}(\mathbf{r}) \approx \mathbf{E}^o(\mathbf{r}) + \left[ i\omega\mu_o \tilde{\mathbf{I}} + \frac{1}{\sigma_o} \nabla \nabla \right] \cdot \tilde{\mathbf{F}}(\mathbf{r}) \cdot \mathbf{E}^o(\mathbf{r}) \quad (8)$$

where

$$\tilde{\mathbf{F}}(\mathbf{r}) = \int_{V_s} d\mathbf{r}' g(\mathbf{r}, \mathbf{r}') \delta\sigma(\mathbf{r}') \tilde{\mathbf{F}}(\mathbf{r}') \quad (9)$$

Note that the first condition cited above could be met by replacing  $\mathbf{E}^o(\mathbf{r})$  in the second term of (8) with  $\mathbf{E}^o(\mathbf{r}_s)$ , where  $\mathbf{r}_s$  is a point within  $V_s$ . This would not give a useful tensor decomposition since it is the regional electric field at the observation point which enters into the MT response function, and leads to the second requirement stated earlier. Note also that the cited conditions can be expected to vary considerably with location. For example, the inductive scale will be much smaller (or the regional field gradient will be much larger) very close to a contact in a 2-D background structure as compared to distant points, and the size of distorting inhomogeneities which can be treated, as well as the ranges over which they can be modeled, using a tensor decomposition can be expected to differ correspondingly. Since the physical dimensions of the inhomogeneity are rarely known a priori, these conditions cannot usually be directly applied, but their violation may explain some instances where tensor decompositions fail.

Equation (8) may be rewritten in the form

$$\mathbf{E}(\mathbf{r}) = \tilde{\mathbf{C}}_3(\mathbf{r}) \cdot \mathbf{E}^o(\mathbf{r}) \quad (10)$$

where the  $3 \times 3$  electric field distortion tensor is given by

$$\tilde{\mathbf{C}}_3(\mathbf{r}) = \tilde{\mathbf{I}} + \left[ i\omega\mu_o \tilde{\mathbf{I}} + \frac{1}{\sigma_o} \nabla \nabla \right] \cdot \tilde{\mathbf{F}}(\mathbf{r}) \quad (11)$$

The elements of  $\tilde{\mathbf{C}}_3$  will be complex unless the inductive terms in (6) or (11) are small compared with the galvanic terms, or equivalently, unless the induction number is substantially less than unity. When this holds, then  $\tilde{\mathbf{C}}_3$  describes galvanic distortion of the electric field. The distortion tensor elements are also functions of position, and the distortion tensor at one point will generally be different from that at another, depending on the geometry of the inhomogeneity. This suggests that the distortion parameters contained in  $\tilde{\mathbf{C}}_3$  are not in themselves inherently interesting, but rather serve as an avenue for estimating the undistorted regional MT response.

At Earth's surface where the normal electric current (and hence normal electric field) vanishes, the vertical and horizontal electric field components are related by

$$\mathbf{E}_z = \mathbf{S}^T \cdot \mathbf{E}_h \quad (12)$$

where  $\mathbf{S}$  is a vector of frequency-independent constants. For example, when the earth-air interface is horizontal, then  $\mathbf{S}$  is null, while it contains the local direction cosines at the observation point in the presence of topography. The electric distortion tensor (11) may be partitioned into

$$\hat{\mathbf{C}}_3 = \begin{bmatrix} \hat{\mathbf{C}}_2 & \vec{\psi} \\ \vec{\Psi}^T & \end{bmatrix} \quad (13)$$

where  $\hat{\mathbf{C}}_2$  is a second rank tensor,  $\vec{\psi}$  is a two-element column vector, and  $\vec{\Psi}^T$  is a three-element row vector. Combining (10) with (12)-(13) yields

$$\mathbf{E}_h(\mathbf{r}) = \hat{\mathbf{C}}(\mathbf{r}) \cdot \mathbf{E}_h^o(\mathbf{r}) \quad (14)$$

where  $\hat{\mathbf{C}}$  is the  $2 \times 2$  tensor describing distortion of the horizontal electric field given by

$$\hat{\mathbf{C}}(\mathbf{r}) = \hat{\mathbf{C}}_2(\mathbf{r}) + \vec{\psi}(\mathbf{r}) \cdot \mathbf{S}^T(\mathbf{r}) \quad (15)$$

Its elements are real under the same conditions as for  $\hat{\mathbf{C}}_3$ : when the inductive terms are small compared to the galvanic ones in (6) or (11). A further caution is required for ocean-based measurements since the normal component of  $\mathbf{E}$  does not necessarily vanish at the seafloor, and hence (12) does not hold exactly. However, the part of oceanic  $\mathbf{E}_z$  due to external sources is typically small compared to the horizontal components when the bottom is relatively flat-lying, and (12) should be satisfied approximately. This could break down in the presence of strong topography where the elements of  $\mathbf{S}$  may be quite frequency-dependent, depending on the underlying conductivity structure.

The derivation of the tensor describing magnetic field distortion is very similar to that for the electric field. Substituting (7) into (4) gives

$$\mathbf{B}(\mathbf{r}) \approx \mathbf{B}^o(\mathbf{r}) + \hat{\mathbf{P}}_3(\mathbf{r}) \cdot \mathbf{E}^o(\mathbf{r}) \quad (16)$$

where

$$\hat{\mathbf{P}}_3(\mathbf{r}) = \mu_o \nabla \times \hat{\mathbf{F}}(\mathbf{r}) \quad (17)$$

The horizontal components of (16) are given by

$$\mathbf{B}_h(\mathbf{r}) = \mathbf{B}_h^o(\mathbf{r}) + \hat{\mathbf{D}}(\mathbf{r}) \cdot \mathbf{E}_h^o(\mathbf{r}) \quad (18)$$

where

$$\hat{\mathbf{D}}(\mathbf{r}) = \hat{\mathbf{P}}_2(\mathbf{r}) + \vec{\xi}(\mathbf{r}) \cdot \mathbf{S}^T(\mathbf{r}) \quad (19)$$

and  $\hat{\mathbf{P}}_3$  has been partitioned like (13), with  $\hat{\mathbf{P}}_2$ ,  $\vec{\xi}$ , and  $\vec{\Xi}^T$  replacing  $\hat{\mathbf{C}}_2$ ,  $\vec{\psi}$ , and  $\vec{\Psi}^T$ , respectively. The remaining vertical component of  $\mathbf{B}$  is given by

$$\mathbf{B}_z(\mathbf{r}) = \mathbf{B}_z^o(\mathbf{r}) + \mathbf{Q}^T(\mathbf{r}) \cdot \mathbf{E}_h^o(\mathbf{r}) \quad (20)$$

where

$$\mathbf{Q}(\mathbf{r}) = \vec{\Xi}_h(\mathbf{r}) + \Xi_z \mathbf{S} \quad (21)$$

and  $\vec{\Xi}_h$  and  $\Xi_z$  are the horizontal and vertical parts of  $\vec{\Xi}$ , respectively. The elements of  $\hat{\mathbf{D}}$  and  $\mathbf{Q}$  will be real under the same conditions as apply to the electric distortion model. Furthermore, the same cautions about applying (18) and (20) to seafloor data must be invoked.

The observed MT response tensor  $\hat{\mathbf{Z}}$  contains four complex elements and is related to the observed electric

and magnetic fields by  $\mathbf{E}_h = \hat{\mathbf{Z}} \cdot \mathbf{B}_h$ . The regional MT response tensor  $\hat{\mathbf{Z}}_2$  is antidiagonal, containing two complex elements since the regional fields are assumed to be due at most to a 2-D structure and satisfies  $\mathbf{E}_h^o = \hat{\mathbf{Z}}_2 \cdot \mathbf{B}_h^o$ . Combining these definitions with (14) and (18) gives

$$\mathbf{E}_h = \hat{\mathbf{C}} \cdot \hat{\mathbf{Z}}_2 \cdot (\hat{\mathbf{I}} + \hat{\mathbf{D}} \cdot \hat{\mathbf{Z}}_2)^{-1} \cdot \mathbf{B}_h \quad (22)$$

so that the observed and model MT response tensors are related by

$$\hat{\mathbf{Z}} = \hat{\mathbf{C}} \cdot \hat{\mathbf{Z}}_2 \cdot (\hat{\mathbf{I}} + \hat{\mathbf{D}} \cdot \hat{\mathbf{Z}}_2)^{-1} \quad (23)$$

where the position dependence of the tensors in (22)-(23) has been omitted. Equation (23) holds in strike coordinates where the observation coordinate system coincides with that of the regional structure; the elements of  $\hat{\mathbf{C}}$  and  $\hat{\mathbf{D}}$  then contain the distortion parameters in the strike reference system. In the galvanic limit where all of the parameters in the distortion tensors are real, the electric field distortion tensor  $\hat{\mathbf{C}}$  has an effect on the observed response which is frequency independent but can result in shifts in the magnitudes and mixing of the phases of the regional 2-D responses. By contrast, the magnetic field distortion tensor  $\hat{\mathbf{D}}$  can change both the magnitudes and phases of the observed response as a function of frequency because it multiplies the complex, frequency-dependent regional response tensor  $\hat{\mathbf{Z}}_2$ . However, the magnetic distortion term  $\hat{\mathbf{D}} \cdot \hat{\mathbf{Z}}_2$  decays with decreasing frequency approximately as  $\omega^{1/2}$  and hence will decline in importance as the frequency drops.

The observed and regional vertical-to-horizontal magnetic field transfer functions satisfy  $\mathbf{B}_z = \mathbf{M}^T \cdot \mathbf{B}_h$  and  $\mathbf{B}_z^o = (\mathbf{M}^o)^T \cdot \mathbf{B}_h^o$ , respectively. Combining these definitions with that for the regional MT response tensor, (18), and (20) yields a relation between the observed and regional magnetic transfer function

$$\mathbf{M}^T = ((\mathbf{M}^o)^T + \mathbf{Q}^T \cdot \hat{\mathbf{Z}}_2) \cdot (\hat{\mathbf{I}} + \hat{\mathbf{D}} \cdot \hat{\mathbf{Z}}_2)^{-1} \quad (24)$$

Note that (24) involves a term additive to the regional magnetic transfer function and proportional to the regional MT response tensor as well as a multiplicative tensor term, while (23) is only a multiplicative tensor relation. This means that the magnetic transfer function decomposition cannot be estimated independent of that for the MT response tensor, a fact which is not surprising given (4).

### Indeterminacy of the Distortion Parameters

By expanding in a Pauli spin matrix basis, Groom and Bailey [1989] showed that the electric galvanic distortion tensor in (14)-(15) can be further decomposed into the product of a scalar and three tensors

$$\hat{\mathbf{C}} = g \hat{\mathbf{T}} \cdot \hat{\mathbf{S}} \cdot \hat{\mathbf{A}} \quad (25)$$

where  $\hat{\mathbf{T}}$ ,  $\hat{\mathbf{S}}$ , and  $\hat{\mathbf{A}}$  are called the twist, shear, and anisotropy tensors, respectively, and each contain a single real scalar parameter in the galvanic limit. Groom and Bailey described the physical meaning of these three tensors, proved that the decomposition is unique under reasonable assumptions about the MT response tensor, and showed that only the twist and shear parameters can be determined from a given MT response tensor. The site gain  $g$

and anisotropy parameter in  $\hat{\mathbf{A}}$  are uniquely determined only if the magnitudes of the two principal responses in  $\hat{\mathbf{Z}}_2$  are independently known at some frequency. This is analogous to the well-known static shift effect in which each of the principal MT responses can be multiplicatively scaled by a real parameter which cannot be estimated without a priori information; the site gain and anisotropy terms replace the usual static shift parameters. Anisotropy caused by the local structure (as described by  $\hat{\mathbf{A}}$ ) cannot be distinguished from regional anisotropy contained in  $\hat{\mathbf{Z}}_2$ , and hence  $\hat{\mathbf{A}}$  may be subsumed into  $\hat{\mathbf{Z}}_2$ . This leaves only the site gain as a free parameter. Thus, the GB electric galvanic distortion decomposition is indeterminate without ancillary information on either the MT response tensor or the actual electrical structure.

The full electric and magnetic distortion decomposition (23) contains additional indeterminacy, as will now be proved. The magnetic distortion tensor may be parameterized as

$$\hat{\mathbf{B}} = \begin{bmatrix} -\gamma & \alpha \\ -\beta & \epsilon \end{bmatrix} \quad (26)$$

where the four parameters are real in the galvanic limit.  $\hat{\mathbf{D}}$  may be expanded into the sum of antidiagonal and diagonal parts  $\hat{\mathbf{D}}_A$  and  $\hat{\mathbf{D}}_D$ . It is easy to show that (23) may be written

$$\hat{\mathbf{Z}} = \hat{\mathbf{C}} \cdot \hat{\mathbf{Z}}'_2 \cdot (\hat{\mathbf{I}} + \hat{\mathbf{B}}_D \cdot \hat{\mathbf{Z}}'_2)^{-1} \quad (27)$$

where  $\hat{\mathbf{Z}}'_2 = \hat{\mathbf{Z}}_2 \cdot (\hat{\mathbf{I}} + \hat{\mathbf{B}}_A \cdot \hat{\mathbf{Z}}_2)^{-1}$ .  $\hat{\mathbf{Z}}_2$  and  $\hat{\mathbf{Z}}'_2$  are not distinguishable since the forms of the tensor decompositions in (23) and (27) are identical. Only the diagonal part of  $\hat{\mathbf{D}}$  in (26) may be estimated from measured MT response functions. Furthermore, in the presence of galvanic distortion of the electric field, the diagonal part of  $\hat{\mathbf{D}}$  can be uniquely estimated only when the site gain  $g$  and local anisotropy  $\hat{\mathbf{A}}$  are known. To see this, substitute (25) into (27) and rewrite the latter as

$$\hat{\mathbf{Z}} = \hat{\mathbf{T}} \cdot \hat{\mathbf{S}} \cdot \hat{\mathbf{Z}}''_2 \cdot (\hat{\mathbf{I}} + \hat{\mathbf{B}}'_D \cdot \hat{\mathbf{Z}}''_2)^{-1} \quad (28)$$

where  $\hat{\mathbf{Z}}''_2 = g \hat{\mathbf{A}} \cdot \hat{\mathbf{Z}}'_2$  and  $\hat{\mathbf{B}}'_D = \hat{\mathbf{B}}_D \cdot \hat{\mathbf{A}}^{-1}/g$ . Again, since the form of (28) is identical to that of (27), neither  $\hat{\mathbf{Z}}'_2$  and  $\hat{\mathbf{Z}}''_2$  nor  $\hat{\mathbf{B}}'_D$  and  $\hat{\mathbf{B}}_D$  may be distinguished without a priori information.

Another interesting type of indeterminacy to the distortion tensor decomposition can be exposed. Define a new matrix  $\hat{\mathbf{W}} = \text{diag}\{e+t, e-t\}$ , where  $e$  and  $t$  are the shear and twist parameters given by *Groom and Bailey* [1989] and in the Appendix. Equation (28) may be rewritten

$$\hat{\mathbf{Z}} = \hat{\mathbf{T}} \cdot \hat{\mathbf{S}} \cdot \hat{\mathbf{W}}^{-1} \cdot \hat{\mathbf{W}} \cdot \hat{\mathbf{Z}}''_2 \cdot (\hat{\mathbf{I}} + \hat{\mathbf{B}}'_D \cdot \hat{\mathbf{W}}^{-1} \cdot \hat{\mathbf{W}} \cdot \hat{\mathbf{Z}}''_2)^{-1} \quad (29)$$

which is not different in form from (28). The tensor  $\hat{\mathbf{T}} \cdot \hat{\mathbf{S}} \cdot \hat{\mathbf{W}}^{-1}$  is symmetric, and *Smith* [1993] shows that this form of the distortion decomposition describes 2-D surface distortion of a regional 2-D structure which is not distinguishable from 3-D surface distortion without ancillary information (e.g., independent knowledge of the geological structure). *Smith* also derives the strike for 2-D distortion by examining the eigenvalues and eigenvectors of the distortion tensor and shows that this is generally different from that given by the GB decomposition or its extensions even though both are estimated from the same data.

The indeterminacy in the electric and magnetic galvanic distortion decomposition can be resolved if the magnitude and phase of each of the principal regional responses are known at some frequency. This is easily demonstrated by multiplying out the elements in  $\hat{\mathbf{Z}}'_2$  to give

$$\hat{\mathbf{Z}}'_2 = \begin{bmatrix} 0 & \frac{g(1+s)a}{1-\beta a} \\ -g(1-s)b & \frac{1-\alpha b}{1-\alpha b} \end{bmatrix} \quad (30)$$

where  $s$  is the anisotropy parameter, and  $a$  and  $-b$  are the regional MT responses (see the Appendix for definitions). In the absence of magnetic distortion, (30) contains the two principal responses scaled by the static shift parameters  $g(1+s)$  and  $g(1-s)$ , respectively, and hence two real parameters suffice to fix the magnitudes of the response at all frequencies. In the presence of magnetic distortion, (30) defines four real equations which, after rearrangement, are linear in the four unknowns  $g(1-s)$ ,  $g(1+s)$ ,  $\alpha$ , and  $\beta$  and can be solved uniquely if  $a$  and  $b$  are specified at some frequency provided that the elements of  $\hat{\mathbf{Z}}'_2$  are not strictly real. Since  $a$  and  $b$  are rarely known a priori at even one frequency, a more practical way to remove the nonuniqueness might involve making the unknown amplitude and phase shifts at each MT site free parameters to be estimated along with the conductivity structure during inversion. A similar procedure to remove ordinary static shift has been described by *Smith and Booker* [1991].

The magnetic transfer function (24) suffers from even more extensive indeterminacy than the MT response tensor, as is easily demonstrated. Expanding the magnetic distortion tensor  $\hat{\mathbf{D}}$  into diagonal and antidiagonal parts, (24) may be rewritten

$$\mathbf{M}^T = ((\mathbf{M}^o)^T + \mathbf{Q}'^T \cdot \hat{\mathbf{Z}}'_2) \cdot (\hat{\mathbf{I}} + \hat{\mathbf{D}}'_D \cdot \hat{\mathbf{Z}}'_2)^{-1} \quad (31)$$

where  $(\mathbf{M}^o)^T = (\mathbf{M}^o)^T \cdot (\hat{\mathbf{I}} + \hat{\mathbf{B}}_A \cdot \hat{\mathbf{Z}}_2)^{-1}$  and  $\mathbf{Q}' = \hat{\mathbf{A}}^{-1} \cdot \mathbf{Q}/g$ . The form of (31) is not distinguishable from that of (24), and hence the regional magnetic transfer function is indeterminate by the same tensor factor as is the regional MT response tensor. Since the nonuniqueness takes the form of a frequency-dependent complex scaling of the regional transfer function controlled by real frequency-independent parameters, it can in principle be resolved if the regional transfer function is known at some frequency, as for the pure MT case. However, noting that  $(\mathbf{M}^o)' = (0, c)^T$  and  $\mathbf{Q} = (q_x, q_y)^T$ , the first term in (31) is a row vector  $(-q_y b, c + q_x a)$ , where  $a$  and  $b$  are the regional MT responses. On the complex plane, only the component of  $c$  perpendicular to  $a$  can be computed, and the part which is in phase gets inextricably mixed up with the MT response. Since  $a$  itself has an indeterminate phase caused by distortion of the horizontal magnetic field, it is not generally possible to know the true phase of  $c$ . It is only possible to separately estimate  $q_x$  and the part of  $c$  which is out of phase with  $a$ , or, alternatively,  $q_x a$  may be subsumed into the complex parameter  $c$ . In either instance, there are only two free parameters in this component of the magnetic transfer functions that are obtainable from data. *Zhang et al.* [1993] recognized this additive indeterminacy in their work on the

magnetic transfer function, and solved for  $c$  and  $q_x a$  by assuming that they are orthogonal.

### Numerical Solution of the Decomposition

The tensor form of the complete electric and magnetic galvanic distortion decompositions for the MT response tensor and magnetic transfer functions may be written as sets of four and two complex nonlinear equations (equations (A10)-(A13) and (A15)-(A16), respectively, in the Appendix). These may in turn be rewritten as sets of eight and four real nonlinear equations and solved in a desired combination for any number of data using standard routine LMDER1 from the MINPACK library, which is based on a modified Levenberg-Marquardt algorithm. This does require analytic computation of the Jacobian derivatives for each equation; the improvement in accuracy justifies the algebraic difficulty. Note also that these equations may be solved either for individual MT sites or, at the penalty of a much larger computational load, simultaneously for a large array of MT stations. In the latter case, the regional azimuth may be assumed common to all of the sites with the remaining distortion parameters reflecting the location dependence inherent to the tensor decomposition.

While the assumption of 3-D local distortion acting on a 2-D inductive response has empirically been observed to be common, it will not be valid in all cases, and it is essential that tests for the appropriateness of the model be devised. *Groom and Bailey* [1989] discuss two approaches: statistical tests for the goodness of fit and examination of the frequency dependence of the distortion parameters. The second of these is based on the premise that the distortion model is realistic when the decomposition parameters are frequency-independent over a range of frequencies; it would not be surprising for a local structure to show inductive effects (and hence a nongalvanic response) at high frequencies, depending on the actual geometry, conductivity, and nature of the coupling between the surface and regional structure. *Groom and Bailey* [1989] and *Groom and Bahr* [1992] show numerous examples, and the general principles they espouse are equally applicable when the magnetic distortion extensions of this paper are made. Of course, conclusions about the appropriateness of a local distortion model are always strengthened if nearby sites with very different measured MT responses give similar regional azimuths and consistent regional responses after decomposition.

A variety of goodness of fit tests have been used for tensor decomposition. *Groom and Bailey* [1989] utilized the root-mean-square relative error of fit, which does not depend on the uncertainties in the measured response functions. However, if the data have been processed robustly (so that they are not biased by heteroscedasticity in the data) and reliable confidence intervals on them are available, then the standard  $\chi^2$  test for goodness of fit is reliable and offers the advantage that significance levels can be estimated easily if the equivalent number of degrees of freedom is known. The latter depends critically on the manner in which the tensor decomposition is applied. There are 8 degrees of freedom in the observed complex MT response data at each frequency and an additional four if the magnetic transfer function is avail-

able. For electric field distortion of the MT response function, a frequency-by-frequency decomposition may be obtained which requires seven parameters (the two complex principal response functions, twist, shear, and regional azimuth), and the  $\chi^2$  test will have a single degree of freedom, so that the expected value of  $\chi^2$  is 1, while the 95% level is 3.84. If the electric field decomposition is applied over broad frequency bands, presuming that frequency independence of the parameters has been established, then each frequency has four degrees of freedom (due to the two complex frequency-dependent principal response functions) less those for the remaining three telluric distortion parameters, which are assumed to be evenly distributed across the band. The latter usually constitutes a small reduction, and hence the degrees of freedom may be assumed to be 4. The expected value of  $\chi^2$  is then approximately 4, and the 95% level is 9.49. However, when magnetic distortion decomposition is included and the decomposition is applied on a frequency-by-frequency basis, there are nine parameters to be estimated from eight MT data, and the problem is formally underdetermined. If the magnetic transfer function is decomposed simultaneously with the MT tensor, there are 12 parameters to be estimated from 12 data, and the fit will be exact. The underdetermined MT magnetic distortion problem can be solved only over frequency bands containing two or more entries. In this instance and when the estimates are independent, each frequency contains 4 degrees of freedom with a slight reduction due to the five distortion parameters which are again assumed to be distributed evenly across the band. Decomposition of the full MT and magnetic transfer function across frequency bands gives 6 degrees of freedom, again less than for the remaining seven parameters distributed across the band. A further caution is required because parameter fitting over frequency bands adds degrees of freedom to the data only when the estimates are independent, a condition which is at best approximate for the MT response tensor at adjacent frequencies due to both estimator- and physics-induced correlation, and erratic results are often achieved unless the bands are sufficiently wide.

Finally, for any tensor distortion decomposition to be useful it is essential not only to correct the response function estimates themselves but also to get meaningful confidence limits on the resulting regional responses. The latter is essential for subsequent modeling of the data, but it is not a simple matter when the transformation is nonlinear. *Groom and Bailey* [1991] decompose the MT tensor using the measured mean responses, then determine the spread of the parameters as the measured values are allowed to vary over the range delimited by their uncertainties. In some instances this yields a statistically indefensible situation where the mean lies outside the inferred error interval. Furthermore, it is unlikely that parametric confidence interval estimation based on the distributions of the tensor decomposition will ever be feasible because those distributions are unknown. Deriving them from the distributions for the response functions, which are a complicated multivariate form of the  $t$ -distribution even for the simplest stationary Gaussian process [Brillinger, 1981], would be hopelessly difficult.

In the field of statistical inference, parametric estimators have been displaced by newer nonparametric types

due to the latter's computational simplicity and better performance in complicated situations. The most frequently used nonparametric method is the jackknife. Application of the jackknife to estimation of the confidence limits on the MT response tensor is described by *Chave and Thomson* [1989], while *Thomson and Chave* [1991] give a complete description of the jackknife in spectral analysis. The jackknife is based on successive resampling with replacement of the available data; these must be independent but not necessarily identically distributed. For example, suppose that the variance of a statistical parameter  $\theta$  is desired (where  $\theta$  may depend in any manner, including nonlinearly, on the data) and that  $N$  data are available. Denote by  $\hat{\theta}_{-i}$  the  $N$  delete-one estimates computed by solving for  $\theta$  after eliminating one data value at a time. Then the jackknife estimate of the variance is

$$\bar{s}^2 = \frac{N-1}{N} \sum_{i=1}^N \left( \hat{\theta}_{-i} - \bar{\theta} \right)^2 \quad (32)$$

where  $\bar{\theta}$  is the arithmetic mean of the delete-one estimates. Confidence intervals on  $\theta$  follow directly from the definition. The computational situation in (32) is slightly more complicated for regression problems because the problem is unbalanced and the solution is vector valued, hence the scalar variance is replaced by a variance-covariance matrix form. The required extensions are discussed by *Chave and Thomson* [1989] and *Thomson and Chave* [1991]. Aside from the computational simplicity seen in (32), the jackknife yields conservative estimates of the variance; *Efron and Stein* [1981] show that the expected value of the jackknife variance slightly exceeds the true variance even when the data are not identically distributed.

Jackknife estimation of the variance of the decomposed response tensor requires saving the delete-one estimates of the measured MT response tensor and magnetic transfer functions. These are computed for each frequency in the measured response tensor by sequentially deleting the raw section Fourier transforms used to estimate the responses, as described by *Chave and Thomson* [1989]. The jackknife estimate of the various galvanic distortion parameters and regional responses then becomes a straightforward solution of the decomposition equations in turn using the delete-one values, followed by application of the multivariate equivalent of (32). Note that this yields the full variance-covariance matrix for the solution. Since it is usually the variances on the regional responses that are of interest rather than those for the distortion parameters, it is computationally expedient to fix the latter at the values obtained with the measured mean responses and jackknife only for the regional response uncertainties. In the absence of magnetic distortion, this reduces the decomposition equations to a linear set which is efficiently solved using QR decomposition rather than a nonlinear equation algorithm.

## Examples and Discussion

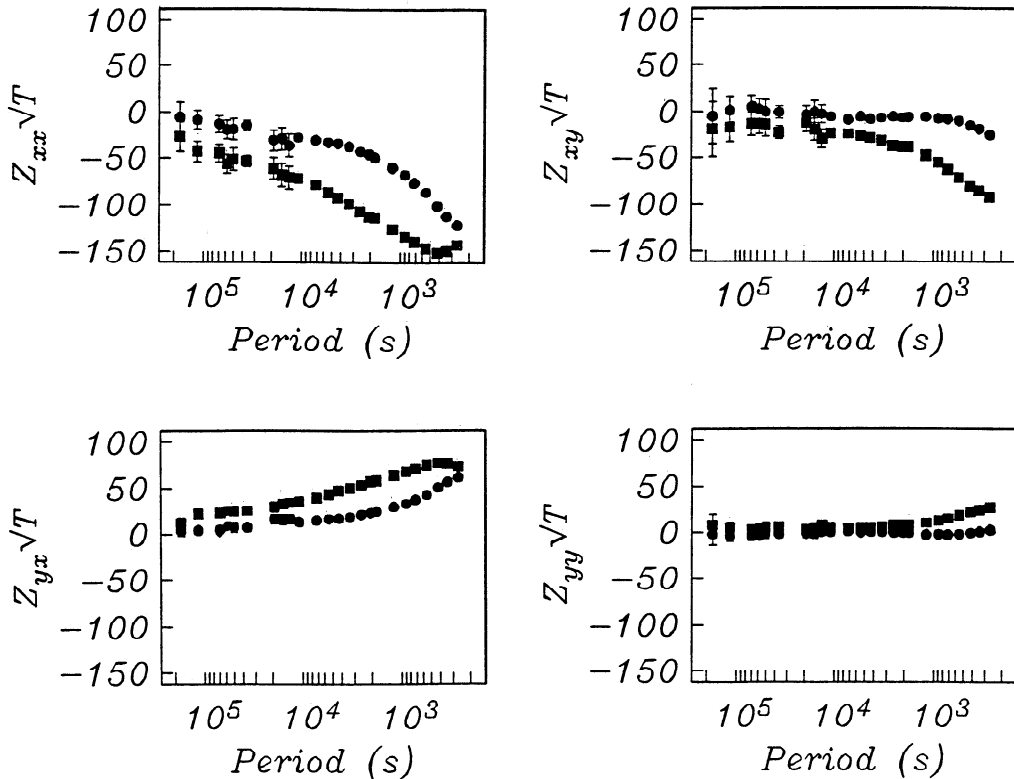
A set of extended period (200–200,000 s) magnetotelluric data were collected using long ( $\approx 1$  km) electrode lines placed at the bottom of Carty Lake ( $48^\circ 10'N$ ,  $82^\circ 42'W$ ) in central Ontario, Canada. A triaxial ringcore

fluxgate magnetometer was buried on the shore of the lake, with a second remote reference unit placed 35 km to the southwest. The field site is located in the Kapsuskaing structural zone which lies within the Superior Province of the central Canadian shield and is characterized by limited sediment cover over crystalline rock. Experimental details and an interpretation of the sounding curve, which is very nearly 1-D in behavior, are given by *Schultz et al.* [1993]. In the present paper, only the galvanic tensor decomposition of the data will be examined in detail.

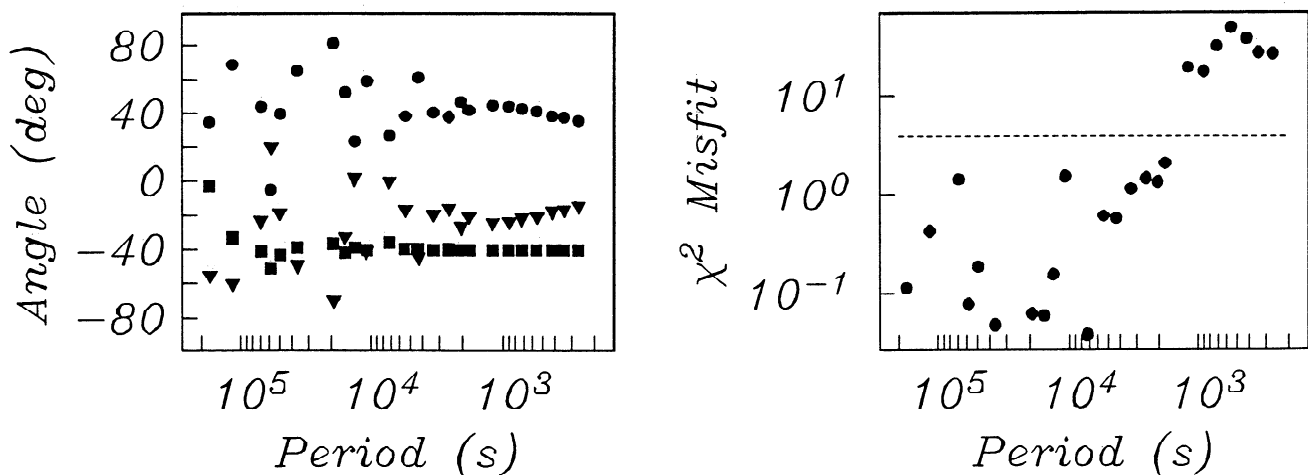
The Carty Lake site is proximal to the auroral zone, and the data exhibit frequent episodes of energetic, non-plane wave source field behavior. Even with robust remote reference processing as described by *Chave and Thomson* [1989], it was not possible to obtain unbiased, minimum phase response functions over any part of the frequency band. This was due to extreme leverage effects from anomalous magnetic field data sections which were usually, but not always, associated with obvious disturbed intervals. Such leverage points are not removable using a conventional robust estimator which detects outliers based on the size of the regression residuals. The problem was solved by extending the robust remote reference algorithm of Chave and Thomson to include data weighting based on a standard statistical measure of leverage [Hoaglin and Welsch, 1978]: comparing the diagonal elements of the hat matrix to their expected values. This resulted in a reduction of the data variance by  $\approx 40\%$ , but the final response tensor is unbiased and minimum phase, and the procedure is statistically justifiable based on the distributions of the final regression residuals and hat matrix diagonal. Further details will be published elsewhere.

Figure 1 shows the four elements of the MT response tensor in geomagnetic coordinates, where the x-axis is pointed north and the y-axis is pointed east. For clarity, the data are presented as real and imaginary parts scaled by  $\sqrt{T}$ . Note that the data scatter increases markedly at periods longer than  $\approx 20,000$  s; this is due to inability to completely remove bias caused by a relatively broadband component of the non-plane wave solar daily variation, a problem which plagues long-period MT [e.g., Egbert et al., 1992]. However, it is apparent that the  $Z_{xx}$  term has a larger magnitude than the antidiagonal response tensor elements over most of the period range, while the  $Z_{yy}$  term is significantly different from zero at periods shorter than 10,000 s. Attempts to diagonalize the tensor using conventional methods fail completely. These data are severely distorted and cannot be interpreted without correction.

The standard electric field galvanic distortion model of *Groom and Bailey* [1989] was fit to the MT response tensor without requiring frequency independence of the decomposition parameters (Figure 2). The resulting  $\chi^2$  misfit was below the 95% confidence threshold at periods longer than  $\approx 1200$  s but much larger ( $> 20$ ) at shorter periods (Figure 3). There is limited variability of the twist and especially the shear at periods shorter than  $\approx 20,000$  s but significantly more fluctuation of the regional azimuth, a phenomenon which is frequently observed with distorted MT data, as documented by *Jones and Groom* [1993]. However, sufficient frequency



**Figure 1.** The four elements of the MT response tensor from the Carty Lake data described in the text. The coordinate system has the x- and y-axes oriented to the geomagnetic north and east, respectively. In each case, the real (solid circles) and imaginary (solid squares) parts along with their 95% jackknife confidence limits are shown scaled by the square root of period. The units of the ordinate are  $\text{mV}\cdot\text{s}^{1/2}\cdot\text{km}^{-1}\cdot\text{nT}^{-1}$ .



**Figure 2.** The twist (solid circles), shear (solid squares), and regional azimuth (solid triangles) for a frequency-by-frequency electric field galvanic distortion model fit to the Carty Lake data of Figure 1. The regional azimuth is the positive clockwise rotation from the observation (geomagnetic) coordinate system to the regional one, while the twist and shear angles are positive clockwise relative to the regional strike.

**Figure 3.** The  $\chi^2$  misfit for the frequency-by-frequency electric field galvanic distortion model whose parameters are shown in Figure 2. Since there are eight data at each frequency, while seven parameters are fit, there is 1 degree of freedom per estimate. The 95% value for the  $\chi^2$  test at 1 degree of freedom is shown as the dashed line. The model fit is not acceptable at periods below  $\approx 1500$  s using a 95% criterion.

independence of the parameters is present to justify attempting to fit a model with invariant twist, shear, and azimuth. The resulting  $\chi^2$  misfit is shown in Figure 4. The twist of  $38.6^\circ$  and shear of  $-40.4^\circ$  are commensurate with the severely distorted nature of the data in Figure 1, while the regional azimuth is  $-18.0^\circ$ . The misfit statistic in Figure 4 clearly indicates that the model is inappropriate at the short-period end of the range; virtually all of the estimates exceed the 95% threshold for 4 degrees of freedom at periods below  $\approx 3000$  s.

Misfit of the electric field galvanic distortion model at relatively short periods but not at longer ones is suggestive of magnetic field galvanic distortion. Accordingly, the full electric and magnetic field galvanic distortion model was applied to the Carty Lake MT response tensor. As discussed earlier, frequency-by-frequency model fits are not possible owing to the underdetermined nature of the problem when magnetic distortion is included. Pairwise model fits are numerically feasible but usually lead to substantial scatter in the parameters which suggests statistical instability, probably due to the high degree of correlation between adjacent frequencies in the MT response estimate. Overlapping three-frequency-wide bands produced more consistent results. This confirmed the suitability of an electric and magnetic galvanic distortion model with frequency-independent elements at periods below a few thousand seconds. To produce a consistent estimate at all periods, the magnetic distortion parameters are first fit to the data at periods shorter than 1200 s where the magnetic galvanic distortion model is appropriate, then fixed to the solution values at all periods while the electric distortion parameters are computed. This produces essentially no change to the decomposed response as compared to the electric only

result at long periods because of the low frequency decrease in the magnitude of  $\mathbf{B} \cdot \mathbf{Z}_2$  in (23). However, (23) constitutes a nonlinear set of equations, and hence interaction of the electric and magnetic distortion parameters is to be expected. This is manifest in the resulting twist parameter, which has increased substantially to  $59.5^\circ$ . The shear is virtually the same at  $-40.1^\circ$ . The regional azimuth is also increased to  $-42.6^\circ$ . Remembering that the MT azimuth is always ambiguous by  $90^\circ$ , this value is consistent with regional fault structures in the area which strike to the geographic northeast. The magnetic distortion parameters  $\gamma$  and  $\varepsilon$  are 0.0042 and 0.0724, respectively, in units of nT-m/ $\mu$ V. The  $\chi^2$  misfit is shown in Figure 5. There are eight data at each frequency, while four frequency-dependent parameters are fit at each together with five parameters spread over all frequencies, and hence there are slightly fewer than 4 degrees of freedom per frequency. The model fit is acceptable at the 95% level, with only one of the 24 values exceeding this threshold.

Figures 6 and 7 compare the principal regional response tensor components obtained from the electric field only and electric plus magnetic field galvanic tensor decompositions whose misfits are shown in Figures 4 and 5. In each case, the dashed lines denote the 95% confidence bounds on the apparent resistivity and phase at the regional strike azimuth. Without correction for static shifts, this corresponds to the most conductive direction for the electric field model, but to the resistive direction for the full electric and magnetic distortion model, reflecting the  $90^\circ$  ambiguity of the strike direction which always prevails in MT. Note the substantial phase splitting and non-parallel apparent resistivity curves at periods below a few thousand seconds for the electric

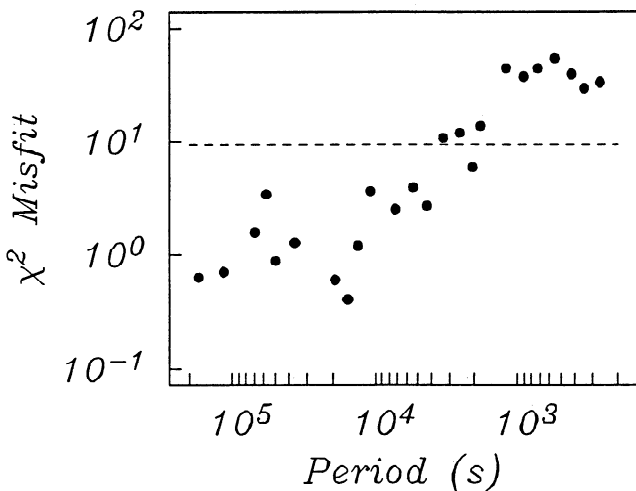


Figure 4. The  $\chi^2$  misfit for the frequency-independent electric field galvanic distortion model of the Carty Lake data as discussed in the text. Since there are eight data at each frequency, while four parameters are fit at each plus three parameters are fit simultaneously at all frequencies, there are slightly fewer than 4 degrees of freedom per estimate. The 95% value for the  $\chi^2$  test at 4 degrees of freedom is shown as the dashed line. The model fit is not acceptable at periods below  $\approx 3000$  s using a 95% criterion.

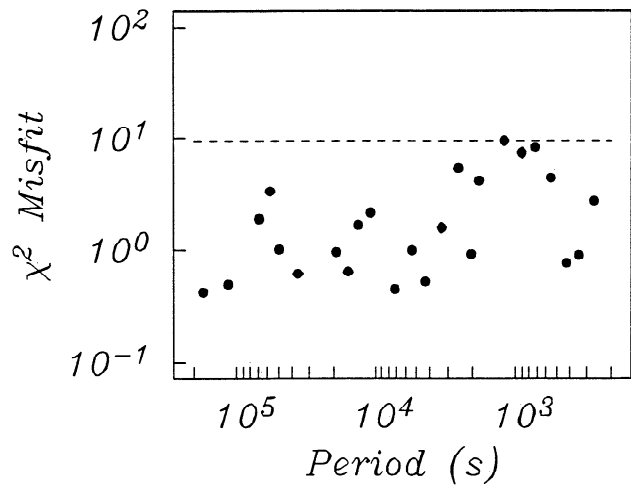
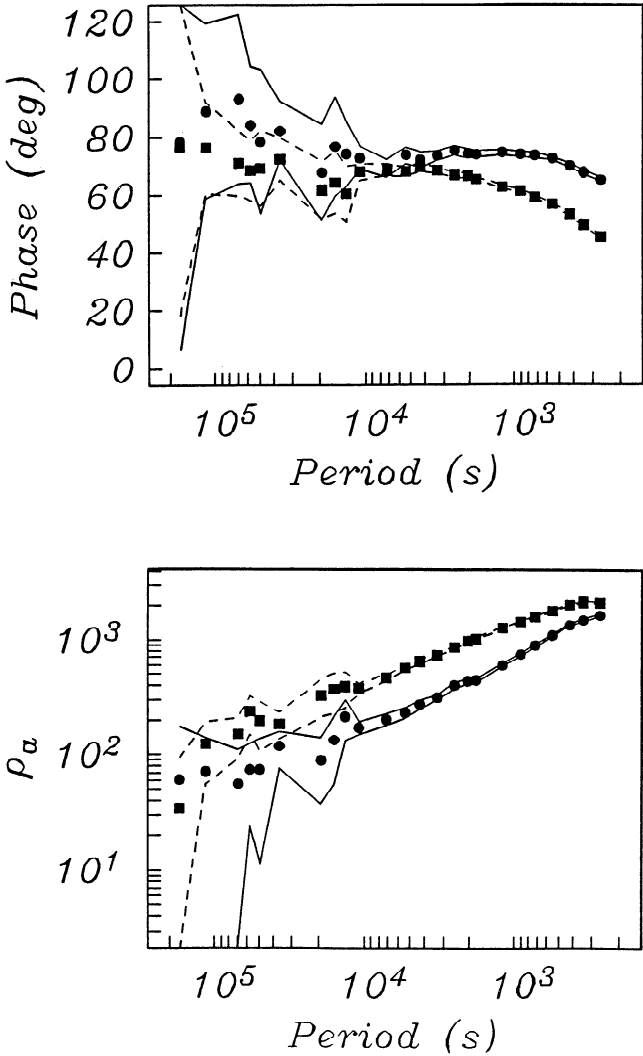


Figure 5. The  $\chi^2$  misfit for the frequency-independent electric and magnetic field galvanic distortion model of the Carty Lake data as discussed in the text. Since there are eight data at each frequency, while four parameters are fit at each plus five parameters are fit simultaneously at all frequencies, there are slightly fewer than 4 degrees of freedom per estimate. The 95% value for the  $\chi^2$  test at 4 degrees of freedom is shown as the dashed line. The model fit is acceptable at all periods using a 95% criterion.



**Figure 6.** The principal apparent resistivities (bottom panel) and phases (top panel) for the electric field galvanic decomposition model of the Carty Lake data whose misfit is shown in Figure 4. The symbols show the mean value of the parameter at each frequency, while the solid and dashed lines show the 95% confidence interval bands computed using the jackknife. The circles correspond to the response element in the direction indicated by the regional strike.

field decomposition in Figure 6. By contrast, inclusion of magnetic field distortion substantially reduces the phase splitting and produces apparent resistivity curves which are parallel over most of the range.

While the combined electric and magnetic distortion model explains the Carty Lake data well, it is also possible to incorporate the magnetic transfer function into the decomposition process. This can be done either by simultaneously solving the magnetic transfer function equations (A15 and A16 in the Appendix) with their MT counterparts or as a separate step using the parameters and regional responses from the MT decomposition. Both of these approaches fail with the Carty Lake data; the statistical misfit is degraded compared to that using only the MT response tensor, and the galvanic distortion

model fails to reproduce the observed magnetic transfer function. Most of the problems occur in the transfer function between the vertical and north magnetic fields. The misfit is due to a persistent bias of the observed transfer function relative to the predicted one. While the cause is not certain, it is probably due to source field effects which are not removed by robust, controlled leverage estimation of the transfer functions. Source effects will certainly be more severe in the magnetic transfer function than in the MT response tensor, and problems in the vertical-to-north magnetic field transfer function are consistent with a source field mechanism. In any case, the magnetic transfer functions are not required to decompose the MT response tensor, as attested to by the acceptable misfit in Figure 5.

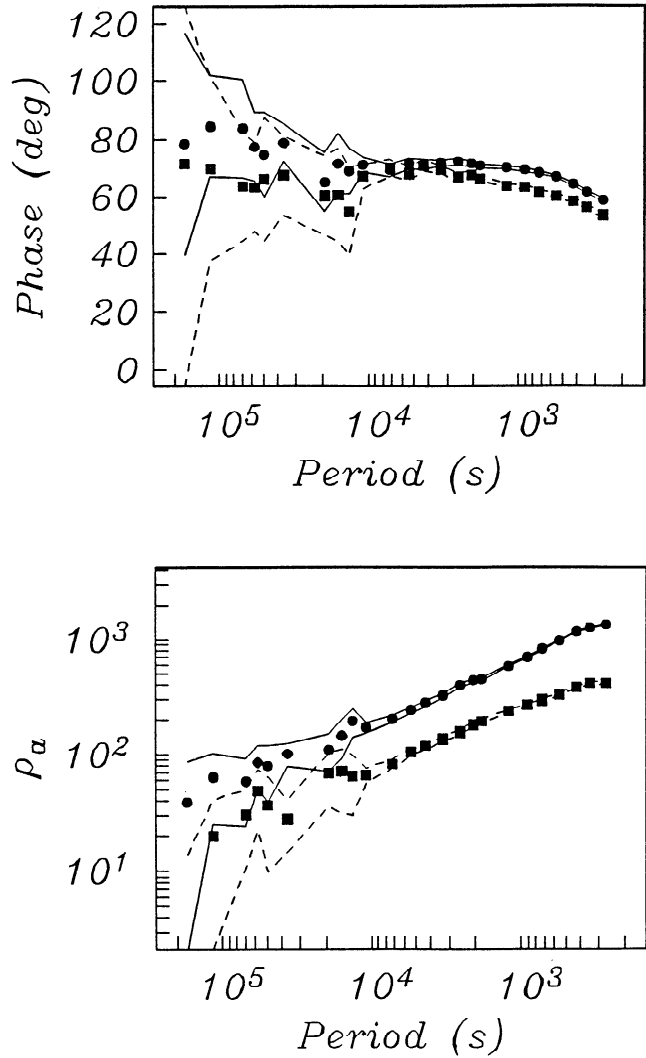


**Figure 7.** The principal apparent resistivities (bottom panel) and phases (top panel) for the electric and magnetic field galvanic decomposition model of the Carty Lake data whose misfit is shown in Figure 5. The symbols show the mean value of the parameter at each frequency, while the solid and dashed lines show the 95% confidence interval bands computed using the jackknife. The circles correspond to the response element in the direction indicated by the regional strike.

On the basis of analyses of data from many sites, magnetic field galvanic distortion appears to be especially important for seafloor MT data, probably because relatively resistive rocks immediately beneath the oceanic crust cause strong electric current concentration and channeling within the highly conductive ocean. A good example is available in the data from site SF3 in the EMSLAB experiment ( $45^{\circ}9.0'N$ ,  $125^{\circ}34.9'W$ ) which were collected on the Juan de Fuca plate seaward of northwestern North America in 1985. Experimental details are reported by Wannamaker *et al.* [1989]. The original time series were reprocessed using the robust, controlled leverage method described previously and a nearby seafloor magnetic field record (site SF4) as a remote reference. Figure 8 shows the frequency-by-frequency electric field galvanic distortion parameter fit to the SF3 data. The parameters are approximately frequency-independent over two bands, with a rather abrupt transition occurring at about the 3000 s period. At the short-period end, the twist and shear are small, while the regional strike is nearly aligned with geographic north (which corresponds to an azimuth of  $0^{\circ}$ ) and the coastline of North America. At the long period end, the twist is essentially unchanged, but the shear is about  $25^{\circ}$  and the regional strike is about  $-40^{\circ}$ . Figure 9 shows the  $\chi^2$  misfit for the distortion decomposition. While the frequency independence of the parameters in Figure 8 certainly suggests the appropriateness of a galvanic distortion model, Figure 9 indicates that its statistical fit is poor, especially in the vicinity of the transition region in Figure 8. The peak value of  $\chi^2$  is in excess of 100. A frequency-independent electric field galvanic distortion model can easily be fit to the data above and below the transition period of Figure 8 with some degradation in the misfit. Comparison of the model to the measured MT response tensor elements shows that most of the misfit

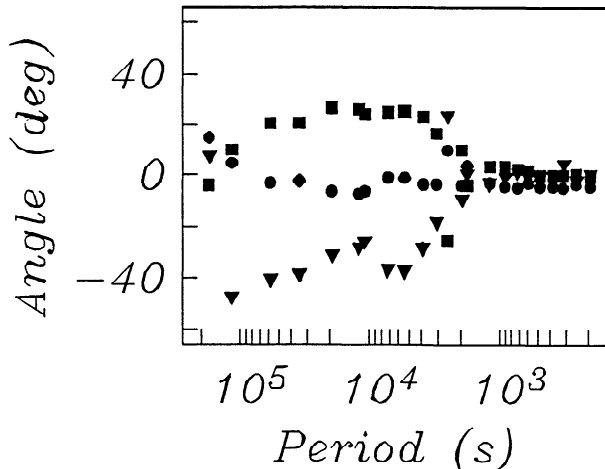


Figure 8. The twist (solid circles), shear (solid squares), and regional azimuth (solid triangles) for a frequency-by-frequency electric field galvanic distortion model fit to the EMSLAB site SF3 data described in the text. The regional azimuth is the positive clockwise rotation from the observation (geographic) coordinate system to the regional one, while the twist and shear angles are positive clockwise relative to the regional strike.

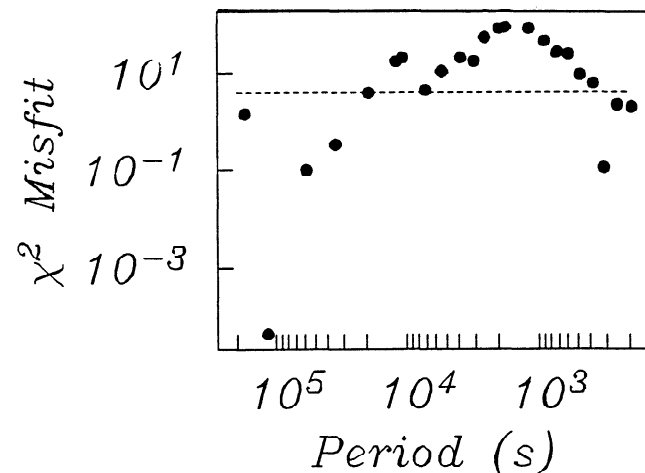


Figure 9. The  $\chi^2$  misfit for the frequency-by-frequency electric field galvanic distortion model whose parameters are shown in Figure 8. Since there are eight data at each frequency, while seven parameters are fit, there is 1 degree of freedom per estimate. The 95% value for the  $\chi^2$  test at 1 degrees of freedom is shown as the dashed line. The model fit is not acceptable at most periods using a 95% criterion.

occurs for the diagonal elements  $Z_{xx}$  and  $Z_{yy}$ . These elements are considerably smaller than their antidiagonal counterparts but remain significantly different from zero over most of their period range.

Figure 10 shows the electric distortion parameters for an electric and magnetic galvanic decomposition of the SF3 data which has been constrained to be separately frequency-independent above and below the transition period seen in Figure 8. Figure 11 shows the correspond-

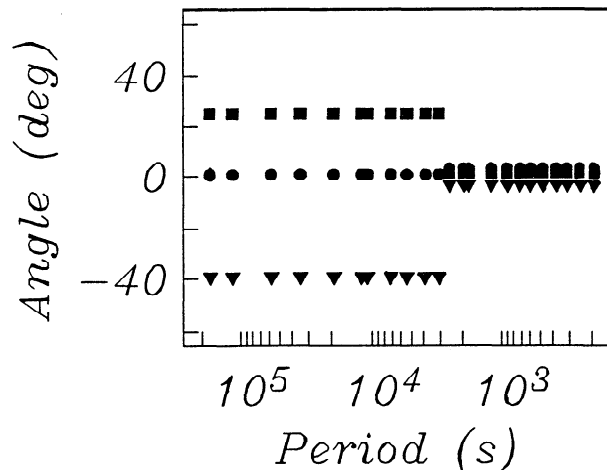


Figure 10. The twist (solid circles), shear (solid squares), and regional azimuth (solid triangles) for a frequency-independent electric and magnetic field galvanic distortion model fit to the EMSLAB site SF3 data described in the text. The regional azimuth is the positive clockwise rotation from the observation (geographic) coordinate system to the regional one, while the twist and shear angles are positive clockwise relative to the regional strike.

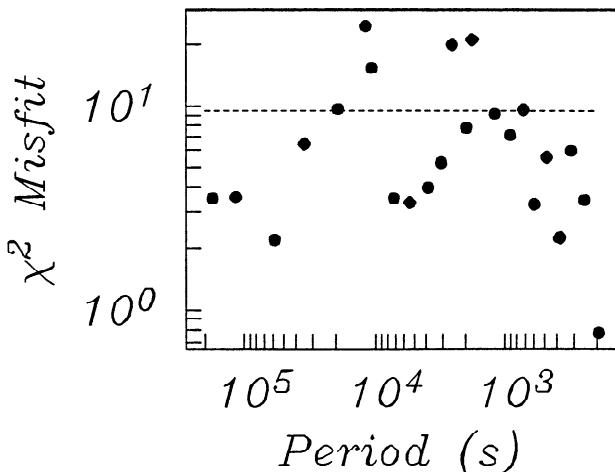


Figure 11. The  $\chi^2$  misfit for the frequency-independent electric and magnetic field galvanic distortion model of the EMSLAB site SF3 data as discussed in the text. Since there are eight data at each frequency, while four parameters are fit at each plus five parameters are fit simultaneously at all frequencies, there are slightly fewer than 4 degrees of freedom per estimate. The 95% value for the  $\chi^2$  test at 4 degrees of freedom is shown as the dashed line. The model fit is acceptable at most periods using a 95% criterion; see text for discussion.

ing misfit statistic. It is clear that the inclusion of magnetic field distortion has greatly improved the fit of the galvanic distortion model by reducing the peak value of  $\chi^2$  by more than a factor of ten. Four of the 23 frequencies still exceed the 95% level for  $\chi^2$ . Of these four values, the two longest period ones are probably contaminated by solar daily variation source fields and are persistently misfit at other EMSLAB sites. The remaining two periods are in the region where the distortion parameters are in transition, where a galvanic distortion model with the given parameters may not be appropriate.

The pattern observed in Figure 9 is also seen at most of the remaining EMSLAB seafloor MT sites, with some weakening of the effect at those close to the Juan de Fuca Ridge. It is relatively simple (if computationally intensive) to fit an electric and magnetic galvanic distortion model simultaneously to many of the seafloor EMSLAB sites by requiring location-specific distortion parameters but a common regional strike. The results are comparable to those shown here. Remembering the 90° ambiguity of the regional azimuth, the long period strike is in approximate alignment with the true spreading direction of the Juan de Fuca plate which is oblique to the ridge axis and trends approximately northeast [Nishimura *et al.*, 1984]. This could be an indication of electrical anisotropy beneath the oceanic lithosphere which is obscured by distortion caused by surface topography. Note also that the distortion parameters shown in Figure 10 are the result of assuming rather than showing that the distortion is caused by a 3-D surficial structure. An alternate hypothesis is that the distortion is caused by a 2-D surface structure. Using the parameterization given by Smith [1993], the long-period twist and shear yield a surficial 2-D distortion direction of -83°, while the short-

period one gives 1.4°. Since there is always a 90° ambiguity in strike direction, these two values are similar to each other and to the strike of the North American coastline. Noting that the transition period occurs where the ocean becomes electrically thin, the long-period decomposition could be treating the ocean as the source of distortion, while the short-period decomposition may be treating the ocean as part of the regional structure. It must be emphasized that these two interpretations of the distortion parameters cannot be distinguished without modeling or tests of consistency using all 10 of the EMSLAB seafloor sites which are at varying distances from the coast.

These examples indicate that galvanic distortion of the magnetic field can be important to periods well in excess of 1000 s in crystalline environments and hence needs to be routinely considered when analyzing many types of long-period MT data. It remains to be seen whether magnetic galvanic distortion is an issue for most wide-band MT data or in sedimentary basins where the surface cover is more uniform and more conductive than in crystalline regions. Furthermore, it is sometimes asserted that the galvanic distortion problem is due to electric field aliasing and that use of the electromagnetic array profiling (EMAP) method [Torres-Verdin and Bostick, 1992], in which the electric field is measured continuously so that spatial filtering methods may be applied, is the best way to remove its influence. This allows only for correction of electric field distortion, and the EMAP method is as susceptible to magnetic field distortion as conventional MT. Thus, a more detailed investigation of magnetic field galvanic distortion using real data from a variety of locales is in order.

#### Appendix: Derivation of the Decomposition Equations

Including a rotation from the observation coordinate system to the regional strike direction, the full distortion tensor decomposition (28) is

$$\hat{\mathbf{Z}} = \hat{\mathbf{R}} \cdot \hat{\mathbf{T}} \cdot \hat{\mathbf{S}} \cdot \hat{\mathbf{Z}}_2 \cdot (\hat{\mathbf{I}} + \hat{\mathbf{D}} \cdot \hat{\mathbf{Z}}_2)^{-1} \cdot \hat{\mathbf{R}}^T \quad (A1)$$

where  $\hat{\mathbf{D}}$  is the diagonal part of the magnetic distortion tensor (26), and the double prime notation on  $\hat{\mathbf{Z}}_2$  in (28) has been dropped. Both the site gain and anisotropy tensor have been subsumed into the regional MT response tensor; this is equivalent to assuming that the site gain  $g$  is unity and the anisotropy factor  $s$  is zero. The rotation matrix is given by

$$\hat{\mathbf{R}} = \begin{bmatrix} \cos\theta & -\sin\theta \\ \sin\theta & \cos\theta \end{bmatrix} \quad (A2)$$

where  $\theta$  is a positive clockwise angle which takes the observation coordinate system to the regional one. The twist tensor is

$$\hat{\mathbf{T}} = \begin{bmatrix} 1 & -t \\ t & 1 \end{bmatrix} \quad (A3)$$

and the shear tensor is

$$\hat{\mathbf{S}} = \begin{bmatrix} 1 & e \\ e & 1 \end{bmatrix} \quad (A4)$$

where  $t$  and  $e$  are the tangents of the electric field twist and shear angles, respectively. The regional MT response tensor is given by

$$\hat{\mathbf{Z}}_2 = \begin{bmatrix} 0 & a \\ -b & 0 \end{bmatrix} \quad (\text{A5})$$

Each of the tensors in (A1) is expanded using a Pauli spin matrix basis, and the multiplications are carried out using the algebra of Pauli spin matrices. Defining four combinations of the measured responses in  $\hat{\mathbf{Z}}$

$$\zeta_0 = Z_{xx} + Z_{yy} \quad (\text{A6})$$

$$\zeta_1 = Z_{xy} + Z_{yx} \quad (\text{A7})$$

$$\zeta_2 = Z_{yx} - Z_{xy} \quad (\text{A8})$$

$$\zeta_3 = Z_{xx} - Z_{yy} \quad (\text{A9})$$

and performing a lot of tedious algebra, the complete electric and magnetic galvanic distortion decomposition reduces to four simultaneous complex nonlinear equations

$$\zeta_0 = \frac{(e+t)a - (e-t)b + (\varepsilon(1-et) - \gamma(1+et))ab}{1-\gamma\epsilon ab} \quad (\text{A10})$$

$$\zeta_1 = \frac{(1-et)a - (1+et)b + (\varepsilon(e+t) - \gamma(e-t))ab}{1-\gamma\epsilon ab} \cos 2\theta \quad (\text{A11})$$

$$\zeta_2 = -\frac{(1-et)a + (1+et)b - (\varepsilon(1-et) + \gamma(1+et))ab}{1-\gamma\epsilon ab} \sin 2\theta \quad (\text{A12})$$

$$\zeta_3 = -\frac{(e+t)a + (e-t)b - (\varepsilon(1-et) + \gamma(1+et))ab}{1-\gamma\epsilon ab} \cos 2\theta \quad (\text{A13})$$

The magnetic transfer function (24) with the same rotation becomes

$$\mathbf{M}^T = ((\mathbf{M}^o)^T + \mathbf{Q}^T \cdot \hat{\mathbf{Z}}_2) \cdot (\hat{\mathbf{I}} + \hat{\mathbf{D}} \cdot \hat{\mathbf{Z}}_2)^{-1} \cdot \hat{\mathbf{R}}^T \quad (\text{A14})$$

where  $(\mathbf{M}^o)^T = (0, c)$  and  $\mathbf{Q}^T = (q_x, q_y)$ . This yields two complex nonlinear equations

$$m_x = \frac{-c}{1-\gamma\epsilon ab} (\sin\theta - \varepsilon b \cos\theta) - \frac{q_y b}{1-\gamma\epsilon ab} (\cos\theta - \gamma a \sin\theta) \quad (\text{A15})$$

$$m_y = \frac{c}{1-\gamma\epsilon ab} (\cos\theta + \varepsilon b \sin\theta) - \frac{q_y b}{1-\gamma\epsilon ab} (\sin\theta + \gamma a \cos\theta) \quad (\text{A16})$$

where  $q_x a$  has been subsumed into  $c$ .

**Acknowledgments.** Our interest in magnetic galvanic distortion has been stimulated by Pascal Tarits' unpublished work showing its importance for seafloor MT. This work was supported by NSF grant OCE91-96236. The Carty Lake data collection was supported by NSF grant EAR88-16998. The authors are grateful for careful reviews by Maurice Tivey, Peter Shaw, Jim Larsen, Ping Zhang, and associate editor Volker Haak. This is WHOI Contribution 8489 and Contribution 3525, Department of Earth Sciences and Institute for Theoretical Geophysics, University of Cambridge.

## References

- Bahr, K., Interpretation of the magnetotelluric impedance tensor: Regional induction and local telluric distortion, *J. Geophys.*, 62, 119-127, 1988.
- Brillinger, D.R., *Time Series: Data Analysis and Theory*, pp. 232-285, Holden-Day, Oakland, Calif., 1981.
- Chave, A.D., and D.J. Thomson, Some comments on magnetotelluric response function estimation, *J. Geophys. Res.*, 94, 14,215-14,225, 1989.
- Efron, B., and C. Stein, The jackknife estimate of variance, *Ann. Stat.*, 9, 586-596, 1981.
- Egbert, G.D., J.R. Booker, and A. Schultz, Very long period magnetotellurics at Tucson Observatory: Estimation of impedances, *J. Geophys. Res.*, 97, 15,113-15,128, 1992.
- Groom, R.W., and K. Bahr, Corrections for near surface effects: Decomposition of the magnetotelluric impedance tensor and scaling corrections for regional resistivities: A tutorial, *Surv. Geophys.*, 13, 341-379, 1992.
- Groom, R.W., and R.C. Bailey, Decomposition of magnetotelluric impedance tensors in the presence of local three-dimensional galvanic distortion, *J. Geophys. Res.*, 94, 1913-1925, 1989.
- Groom, R.W., and R.C. Bailey, Analytic investigations of the effects of near-surface three-dimensional galvanic scatterers on MT tensor decompositions, *Geophysics*, 56, 496-518, 1991.
- Habashy, T.M., R.W. Groom, and B.R. Spies, Beyond the Born and Rytov approximations: A nonlinear approach to electromagnetic scattering, *J. Geophys. Res.*, 98, 1759-1775, 1993.
- Hoaglin, D.C., and R.E. Welsch, The hat matrix in regression and ANOVA, *Am. Stat.*, 32, 17-22, 1978.
- Jiracek, G.R., Near-surface and topographic distortions in electromagnetic induction, *Surv. Geophys.*, 11, 163-203, 1990.
- Jones, A.G., and R.W. Groom, Strike-angle determination from the magnetotelluric impedance tensor in the presence of noise and local distortion: Rotate at your peril!, *Geophys. J. Int.*, 113, 524-534, 1993.
- Larsen, J.C., Low frequency (0.1-6.0 cpd) electromagnetic study of deep mantle electrical conductivity beneath the Hawaiian Islands, *Geophys. J. R. Astron. Soc.*, 43, 17-46, 1975.
- Larsen, J.C., Removal of local surface conductivity effects from low frequency mantle response curves, *Acta Geod. Geophys. Mont.*, 12, 183-186, 1977.
- Nishimura, C., D.S. Wilson, and R.N. Hey, Pole of rotation analysis of present-day Juan de Fuca plate motion, *J. Geophys. Res.*, 89, 10,283-10,290, 1984.
- Schultz, A., R. Kurtz, A.D. Chave, and A.G. Jones, Conductivity discontinuities in the upper mantle beneath a stable craton, *Geophys. Res. Lett.*, in press, 1993.
- Smith, J.T., Understanding telluric distortion matrices, *Geophys. J. Int.*, submitted, 1993.
- Smith, J.T., and J.R. Booker, Rapid inversion of two- and three-dimensional magnetotelluric data, *J. Geophys. Res.*, 96, 3905-3922, 1991.
- Tarits, P., A.D. Chave, J.H. Filloux, and A. Terra, Electromagnetic study of the Tahiti hotspot, paper presented at 17th General Assembly of the European Geophysical Society, Edinburgh, Scotland, April 6-10, 1992.
- Thomson, D.J., and A.D. Chave, Jackknifed error estimates for spectra, coherences, and transfer functions, in *Advances in Spectrum Analysis and Array Processing*, vol. 1, edited by S. Haykin, pp. 58-113, Prentice-Hall, Englewood Cliffs, N.J., 1991.
- Torres-Verdin, C., and F.X. Bostick, Jr., Principles of spatial surface electric field filtering in magnetotellurics: Electromagnetic array profiling (EMAP), *Geophysics*, 57, 603-622, 1992.

- Wannamaker, P.E., G.W. Hohmann, and S.H. Ward, Magnetotelluric responses of three-dimensional bodies in layered earths, *Geophysics*, **49**, 1517–1533, 1984.
- Wannamaker, P.E., et al., Magnetotelluric observations across the Juan de Fuca subduction system in the EMSLAB project, *J. Geophys. Res.*, **94**, 14,111–14,125, 1989.
- Yaghjian, A.D., Electric dyadic Green's functions in the source region, *Proc. IEEE*, **68**, 248–263, 1980.
- Zhang, P., R.G. Roberts, and L.B. Pedersen, Magnetotelluric strike rules, *Geophysics*, **52**, 267–278, 1987.
- Zhang, P., L.B. Pedersen, M. Mareschal, and M. Choteau, Channeling contribution to tipper vectors: A magnetic equivalent to electrical distortion, *Geophys. J. Int.*, **113**, 693–700, 1993.

---

A. D. Chave, Woods Hole Oceanographic Institution, Woods Hole, MA 02543. (tel 508-457-2000x2833, fax 508-457-2150, e-mail: alan@faraday.whoi.edu)

J. T. Smith, Institute of Theoretical Geophysics, Department of Earth Sciences, University of Cambridge, Cambridge CB2 3EQ, England. (tel +44-223-33-44-85, fax +44-223-33-34-50, e-mail: torquil@itg.esc.cam.ac.uk)

(Received August 2, 1993; revised November 19, 1993; accepted November 29, 1993.)